

# Linear Quadratic Regulator Steady-State Cornering Control

Danielle White

**Abstract**—Cornering at the limits of slip is a useful control problem for both student competitions like Formula SAE Electric and commercial road vehicles. This project focuses on control of a vehicle at steady state cornering using both infinite-horizon linear quadratic regulator (LQR) techniques and finite-horizon LQR combined with direct collocation trajectory planning. Infinite-horizon LQR can effectively maintain the cornering equilibrium, but performs poorly in when perturbed from steady state. Direct collocation trajectory planning and finite-horizon LQR are introduced to ameliorate this issue with limited success.

## I. INTRODUCTION

In the Formula SAE Electric (FSAE) student competition, university teams compete build electric formula-style vehicles to compete in a series of dynamic events that test vehicle performance. Although the competition is not autonomous, vehicles still benefit from control algorithms to enhance performance. In particular, two dynamic events (Acceleration and Skidpad) restrict the vehicle to either longitudinal or steady-state lateral acceleration. These conditions allow assumptions that simplify control design. In particular, this project focuses on control for the skidpad event. Specifically, the goal of this project is to produce a control strategy to regulate the vehicle to the optimal steady-state cornering equilibrium around the circular skidpad track. This requires operating at the traction limits of the tires.

Outside of the realm of FSAE, such a controller still has applications: traction control strategies in commercial vehicles provide provide important safety benefits, but traditional approaches center on limiting the tire to its linear regime and do not control at the limits of slip. Control at the limits of slip may allow vehicles to avoid collisions that they would otherwise be inevitable, and ultimately may allow autonomous vehicles to safely operate under more conditions as well.

## II. VEHICLE MODEL

I use a bicycle model with no load transfer effects and a linear tire model, meaning tire lateral and longitudinal tire forces are proportional to slip angle or slip ratio, respectively. The dynamics do not account for the slip limit that exists in real tires, but the control scheme takes this into account, because it attempts to not exceed a given maximum slip angle or slip ratio.

### A. State Dynamics

The state vector of the system is modeled by the following state vector:

$$\mathbf{x} = \begin{bmatrix} r \\ \dot{r} \\ \hat{\theta} \\ \phi \\ \dot{\phi} \end{bmatrix} \quad (1)$$

Here,  $r$  and  $\theta$  represent the position of the vehicle in polar coordinates, and  $\phi$  represents the orientation of the vehicle relative to  $\hat{\theta}$ , as shown in Fig. 1. The angle  $\theta$  is not included in this state vector because will not remain constant even during uniform circular motion, while the rest of these quantities will.

The inputs to the system are front slip ratio  $\kappa_F$ , rear slip ratio  $\kappa_R$ , and steering angle  $\delta$ :

$$\mathbf{u} = \begin{bmatrix} \kappa_F \\ \kappa_R \\ \delta \end{bmatrix} \quad (2)$$

Summing all the tire forces in the  $\hat{\theta}$  and  $\hat{r}$  expressions (and taking care to use the correct components of acceleration in polar coordinates), we find the following equations of motion:

$$\ddot{r} = \frac{F_x \sin \phi + F_y \cos \phi}{m} + r\dot{\theta}^2 \quad (3)$$

$$\ddot{\theta} = \frac{F_x \cos \phi - F_y \sin \phi}{mr} - \frac{2\dot{r}\dot{\theta}}{r} \quad (4)$$

$m$  is the mass of the car, and  $F_x$  and  $F_y$  represent the total tire forces in the longitudinal ( $x$ ) and lateral ( $y$ ) directions,

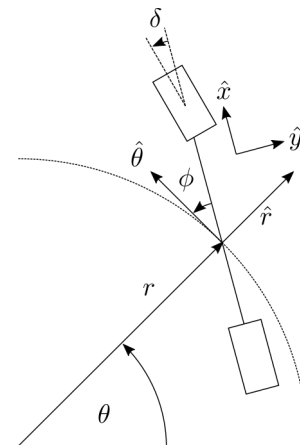


Fig. 1. Coordinate system used for dynamics, along with vehicle frame axes  $x$  and  $y$

respectively. We can express these forces in terms of their front tire ( $F_{xf}$  or  $F_{xf}$ ) and rear tire ( $F_{xr}$  or  $F_{xr}$ ) components:

$$F_x = F_{xf} + F_{xr} \quad (5)$$

$$F_y = F_{yf} + F_{yr} \quad (6)$$

These components can be related to slip ratio  $\kappa$  or slip angle  $\alpha$ :

$$F_x = S_{FL}\kappa_F \sin \delta + S_{FC}\alpha_F \cos \delta + S_{RC}\alpha_R \quad (7)$$

$$F_y = S_{FL}\bar{\kappa}_F \cos \bar{\delta} - S_{FC}\bar{\alpha}_F \sin \bar{\delta} + S_{RL}\bar{\kappa}_R \quad (8)$$

The coefficients  $S_{.L}$  are the longitudinal stiffnesses of the front and rear tires and  $S_{.C}$  are the cornering stiffnesses.

Next, consider the yaw moment about the vehicle. Let  $\psi$  be the heading of the vehicle with respect to x-axis in the inertial frame. Then the yaw moment about the  $z$ -axis describes  $\ddot{\psi}$ :

$$I_z \ddot{\psi} = \ell_R F_{ry} - \ell_F F_{fy} \quad (9)$$

$I_z$  is the moment of inertia of the vehicle about its  $z$  axis, and  $\ell_F$  and  $\ell_R$  are the distances from the front and rear axles to the center of mass, respectively.

We can relate  $\psi$  to  $\phi$  as follows, as shown in Fig 2:

$$\psi = \pi/2 + \theta - \phi \quad (10)$$

Taking second derivatives and substituting terms from (9), we find an equation of motion describing  $\phi$ :

$$\ddot{\phi} = \ddot{\theta} - (\ell_R F_{ry} - \ell_F F_{fy}) / I_z \quad (11)$$

From (3), (4), and (11), we can fully describe the state dynamics in terms of slip inputs. Although this matches the longitudinal inputs, we need expressions for the  $\alpha$  values. Let  $\beta$  represent the body slip angle of the vehicle. It can be calculated as follows (using the components of velocity in polar coordinates):

$$\beta = \arctan \left( \frac{\dot{r}}{r\dot{\theta}} \right) \quad (12)$$

As shown in Fig 3, we can relate  $\beta$  to  $\alpha_F$  and  $\alpha_R$  using  $\phi$ :

$$\alpha_F = \phi - \delta - \beta \quad (13)$$

$$\alpha_R = \phi - \beta \quad (14)$$

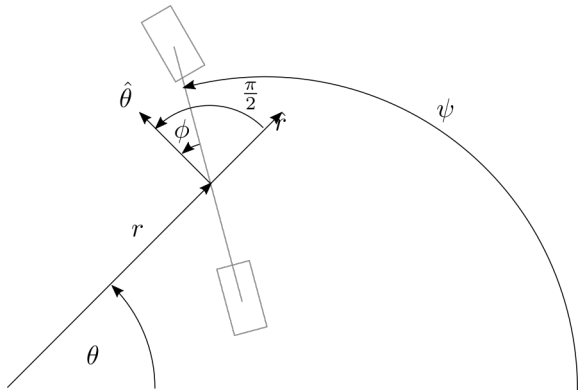


Fig. 2. Relationship between  $\psi$ ,  $\phi$ , and  $\theta$

At this point, given the state inputs, we could fully describe the dynamics of the system.

### B. Steady-state Cornering Conditions

The goal of this section is to find constant values of the state variables and inputs that result in  $\dot{\mathbf{x}} = \mathbf{0}$  and satisfy the conditions of uniform circular motion. Specifically, Uniform circular motion is defined by a constant  $r$  and  $\dot{\theta}$ , which we will call  $\bar{r}$  and  $\bar{\omega}$ . For the dynamics to evaluate to zero,  $\dot{\phi}$  must be 0, so there is also a constant  $\bar{\phi}$ .

Using these steady-state values, we can solve (3) and (4) for the steady state values of  $F_x$  and  $F_y$ :

$$\bar{F}_x = -m\bar{r}\bar{\omega}^2 \sin \bar{\phi} \quad (15)$$

$$\bar{F}_y = -m\bar{r}\bar{\omega}^2 \cos \bar{\phi} \quad (16)$$

Plugging in (7) and (8), we can get expressions for the steady state inputs  $\bar{\kappa}_F$  and  $\bar{\kappa}_R$ :

$$\bar{\kappa}_F = -\frac{S_{RC}\bar{\alpha}_R + S_{FC}\bar{\alpha}_F \cos \bar{\delta} - \bar{F}_y}{S_{FL} \sin \bar{\delta}} \quad (17)$$

$$\bar{\kappa}_R = -\frac{S_{FL}\bar{\kappa}_F \cos \bar{\delta} - S_{FC}\bar{\alpha}_F \sin \bar{\delta} - \bar{F}_x}{S_{RL}} \quad (18)$$

Here  $\bar{\delta}$  is the steady-state steering angle, and  $\bar{\alpha}_R$  and  $\bar{\alpha}_F$  are the steady-state slip angles. Note that in uniform circular motion, since the vehicle's velocity points completely in the  $\hat{\theta}$  direction,  $\beta = 0$ , so  $\bar{\alpha}_R = \bar{\phi}$  and  $\bar{\alpha}_F = \bar{\phi} - \bar{\delta}$ .

The final equation of motion to solve is the yaw moment. Substituting the values we have already found yields this:

$$0 = \frac{S_{RC}\bar{\phi}(\ell_R + \ell_F)}{\ell_F} + m\bar{r}\bar{\omega}^2 \cos \phi \quad (19)$$

How we proceed from this equation depends on what steady-state values we want to specify. Given that the intended application of this controller is on a fixed radius track, we need to be able to specify  $\bar{r}$ .  $\bar{\omega}$  determines how fast the vehicle completes the event (which is ultimately what we want to optimize), while  $\bar{\phi}$  has little impact directly in terms of

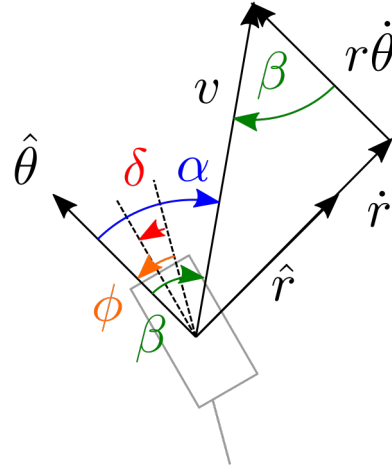


Fig. 3. Relationship between  $\alpha$ ,  $\beta$ , and  $\phi$

performance. Thus, we will proceed solving for  $\bar{\phi}$ . Although (19) cannot be solved for  $\bar{\phi}$  analytically, numerical root finding techniques, such as Brent’s method, can find  $\bar{\phi}$ .

In summary, to find steady state cornering conditions, we first specify  $\bar{r}$ ,  $\bar{\omega}$ , and  $\bar{\delta}$ . Next, we solve for  $\bar{\phi}$  using (19), which also tells us  $\bar{\alpha}_R$  and  $\bar{\alpha}_F$ . Finally, we solve for  $\bar{\kappa}_F$  and then  $\bar{\kappa}_R$  using (15), (16), (17), and (18).

### III. CONTROL

This section examines two control strategies: infinite-horizon linear quadratic regulator (LQR) about the steady-state equilibrium described in section II-B, and a trajectory planner to return to that equilibrium using direct collocation to generate the trajectory that was then stabilized using a finite-horizon linear quadratic regulator. The second control strategy was developed to remedy the poor performance of the first strategy in the face of even minor perturbations from the equilibrium and to explore the effect of slip constraints on performance. Both strategies were implemented and tested using Drake.

#### A. Infinite-horizon LQR

Using Drake’s built-in LQR routines, an LQR controller was generated using the following weights:

$$\mathbf{Q} = \begin{bmatrix} 100 & 0 & 0 & 0 & 0 \\ 0 & 10 & 0 & 0 & 0 \\ 0 & 0 & 10 & 0 & 0 \\ 0 & 0 & 0 & 100 & 0 \\ 0 & 0 & 0 & 0 & 1 \end{bmatrix} \quad (20)$$

$$\mathbf{R} = \begin{bmatrix} 0.5 & 0 & 0 \\ 0 & 0.5 & 0 \\ 0 & 0 & 0.1 \end{bmatrix} \quad (21)$$

When starting at the equilibrium, the LQR controller alone regulates maintains the equilibrium, as shown in Fig 4 and Fig 5. The controller can also tolerate reasonably large disturbances and remain stable, as show in Fig 6 and Fig 7 as well as in Table I, which shows the response of the controller to initial conditions off from equilibrium. (All units are SI units and/or radians, depending on the quantity, and the equilibrium used was  $\bar{r} = 20$ ,  $\bar{\omega} = 0.3$ , and  $\bar{\delta} = 0.1$ ) The price for this is that errors from the desired equilibrium often persist, because higher gains that would remove that error push the system towards instability. Additionally, values much above the ones showed in this table would still cause the vehicle to disturb from the equilibrium as shown in Fig 8 and Fig 9.

TABLE I  
DISTURBANCE REJECTION OF INFINITE-HORIZON LQR

Variable	Disturbance	Remaining disturbance
$r$	-3	-2.19
$\dot{r}$	0.5	0.01858
$\dot{r}$	-0.1	0.00197
$\dot{\theta}$	-0.1	-0.17507
$\dot{\theta}$	0.5	0

#### B. Trajectory Planning with LQR

To remedy this instability, a trajectory planner using direct collocation was added. The solver was constrained to end in at the equilibrium position with the equilibrium input and to not exceed a maximum slip angle. Finite-horizon LQR was used to follow this trajectory. Under some conditions, this control strategy allowed to vehicle to reach equilibrium, as shown in Fig 10 and Fig 11. However, the trajectories generated in this method were erratic and difficult to sustain, as shown in Fig 12, so divergence was still an issue for a wide range of initial conditions. This is likely due to the nonlinear nature of the dynamics.

### IV. CONCLUSIONS

The infinite-horizon LQR controller can maintain equilibrium under certain conditions, but fine-tuning the LQR gains would likely improve performance. The erratic trajectories generated with the trajectory planner remain obstacles before the practical application of that element of the controller. Possible solutions might include experimenting with simplifying assumptions in the dynamics (so that the problem can be solved using quadratic programming instead of a general solver).

Additional modeling considerations would improve the real-world performance of these controllers. Accounting for longitudinal load transfer, using a two-track model (and accounting for lateral load transfer), or using a more advanced tire model that includes load sensitivity or other factors would all improve the fidelity of the model.

One compromise between a linear tire model and the true nonlinear relationship between slip and force would be a piecewise-linear model. Combined with a mode schedule, this would balance computational complexity and model fidelity. Given the simplicity of this control problem, a mode schedule may be feasible.

### V. CODE

Python code used to simulate these control strategies can be found on GitHub:

<https://github.com/daniwhite/SkidpadControl>

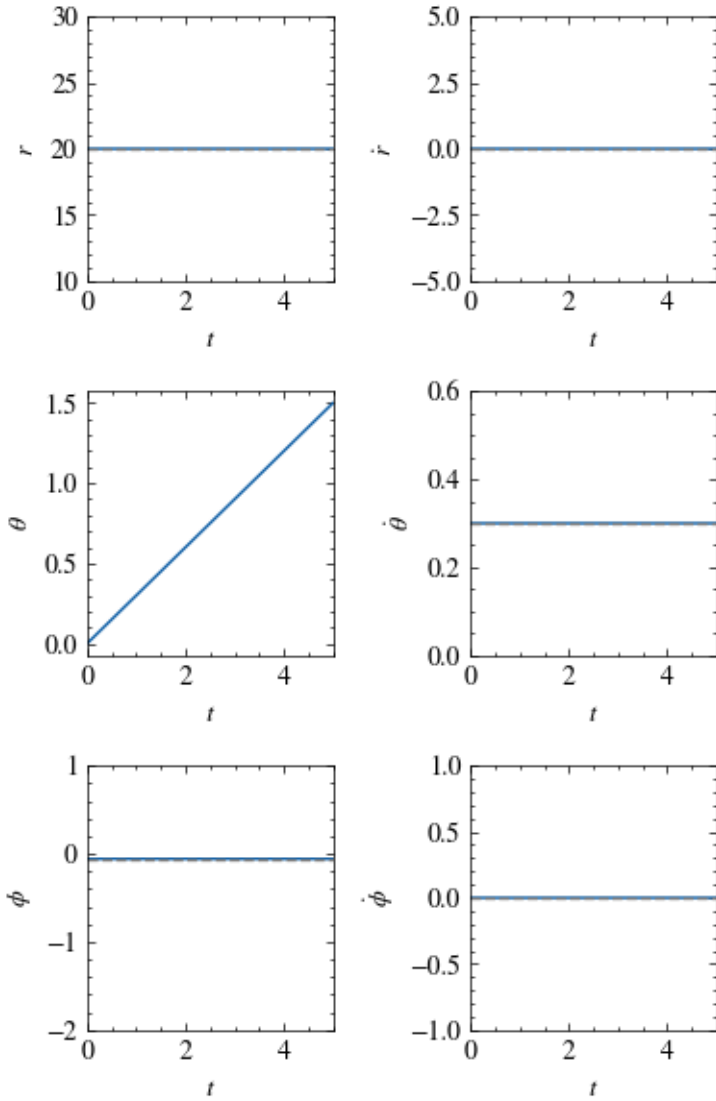


Fig. 4. Time series plots of state variables when system uses infinite-horizon LQR and starts at the equilibrium  $\bar{x} = [20 \ 0 \ 0.3 \ \bar{\phi} \ 0]^T$  (where  $\bar{\phi}$  is the corresponding steady-state  $\phi$  value). Note that all remain constant except for  $\theta$ , which is the only variable which changes during steady state cornering.

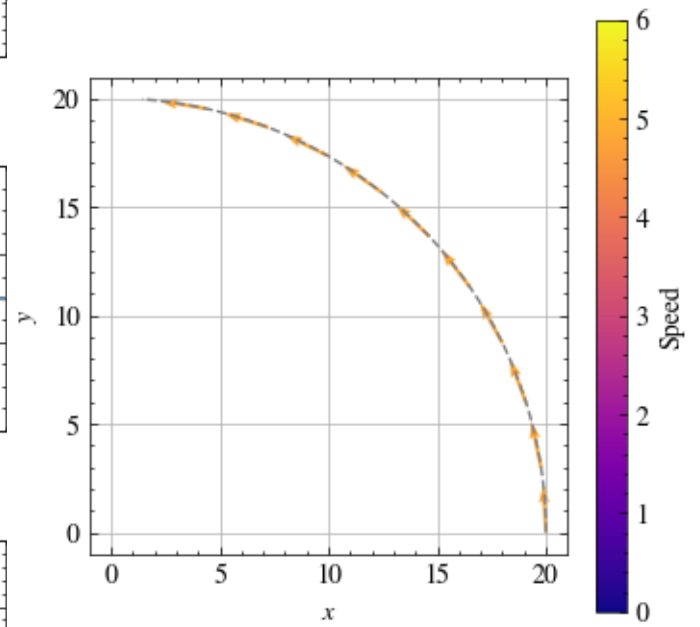


Fig. 5. Vehicle trajectory when system infinite-horizon LQR and starts at equilibrium. The vectors represent vehicle orientation (so they point in the vehicle's longitudinal direction), and their color represents the vehicle speed. Also, note that  $x$  and  $y$  here simply represent Cartesian coordinates, not  $\hat{x}$  or  $\hat{y}$  in the vehicle's frame.

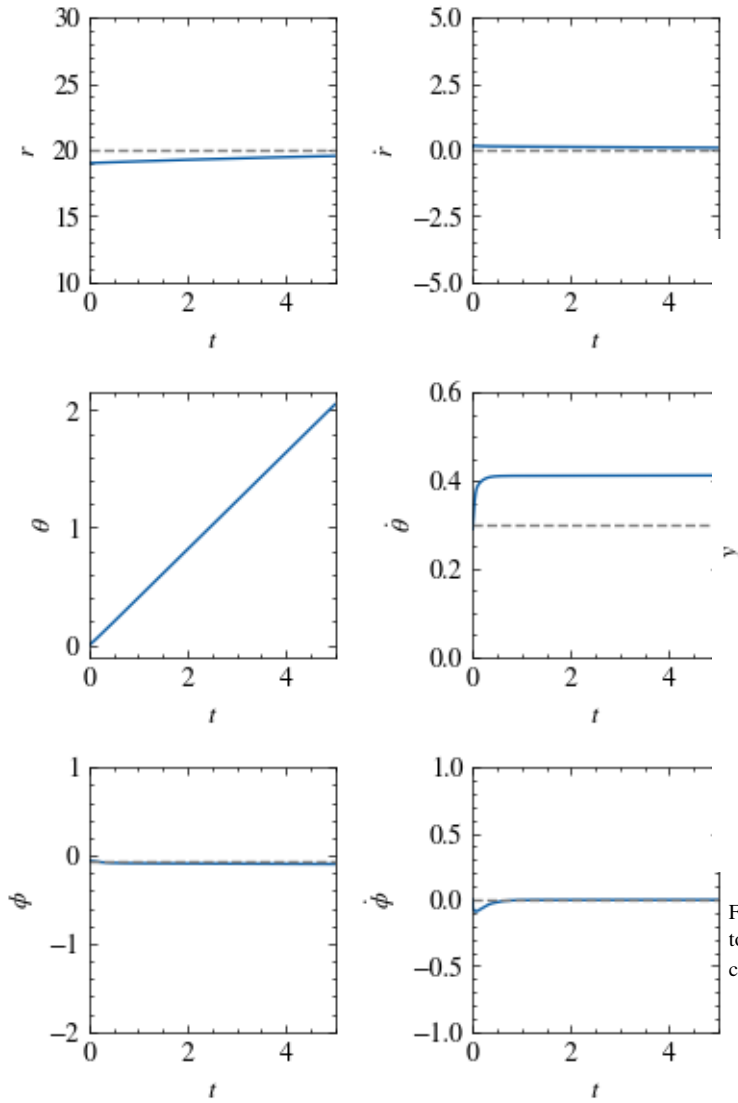


Fig. 6. Time series plots of state variables when system uses infinite-horizon LQR regulating to the equilibrium  $\bar{\mathbf{x}} = [20 \ 0 \ 0.3 \ \bar{\phi} \ 0]^T$  and has the initial conditions  $\bar{\mathbf{x}} = [19 \ 0.1 \ 0.29 \ \bar{\phi} \ 0]^T$ .

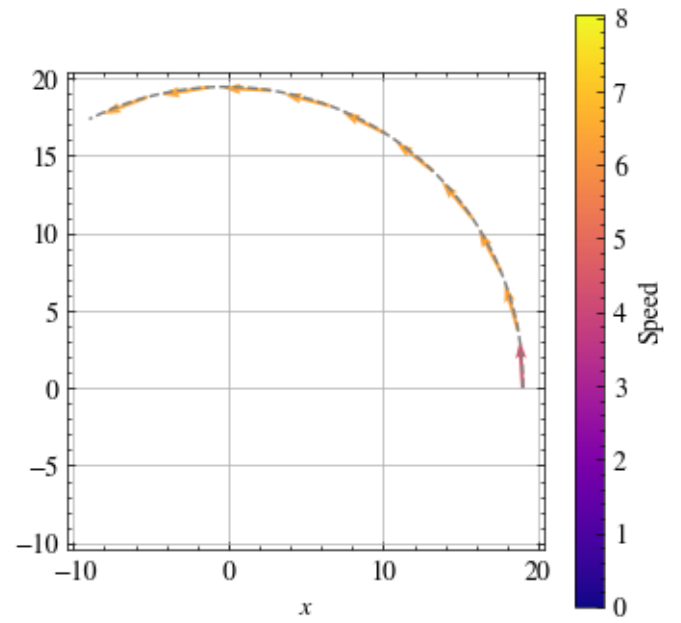


Fig. 7. Vehicle trajectory when system uses infinite-horizon LQR regulating to the equilibrium  $\bar{\mathbf{x}} = [20 \ 0 \ 0.3 \ \bar{\phi} \ 0]^T$  and has the initial conditions  $\bar{\mathbf{x}} = [19 \ 0.1 \ 0.29 \ \bar{\phi} \ 0]^T$ .

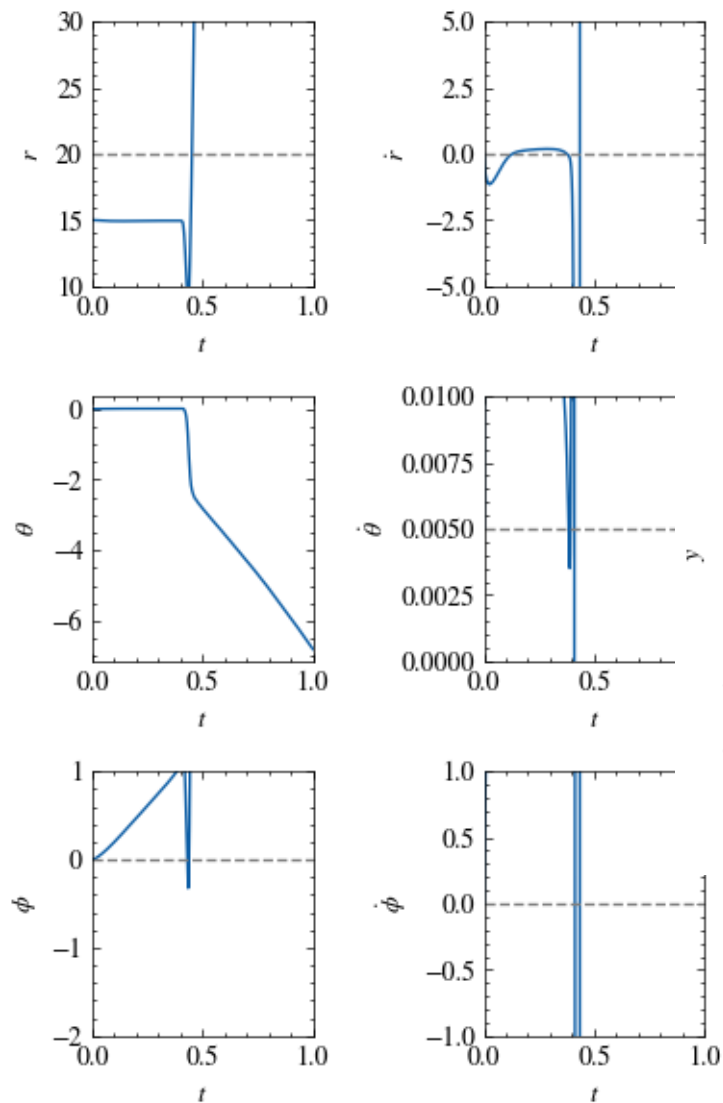


Fig. 8. Time series plots of state variables when system uses infinite-horizon LQR regulating to the equilibrium  $\bar{\mathbf{x}} = [20 \ 0 \ 0.3 \ \bar{\phi} \ 0]^T$  and has the initial conditions  $\bar{\mathbf{x}} = [15 \ 0 \ 0.3 \ \phi_{bar} \ 0]^T$ .

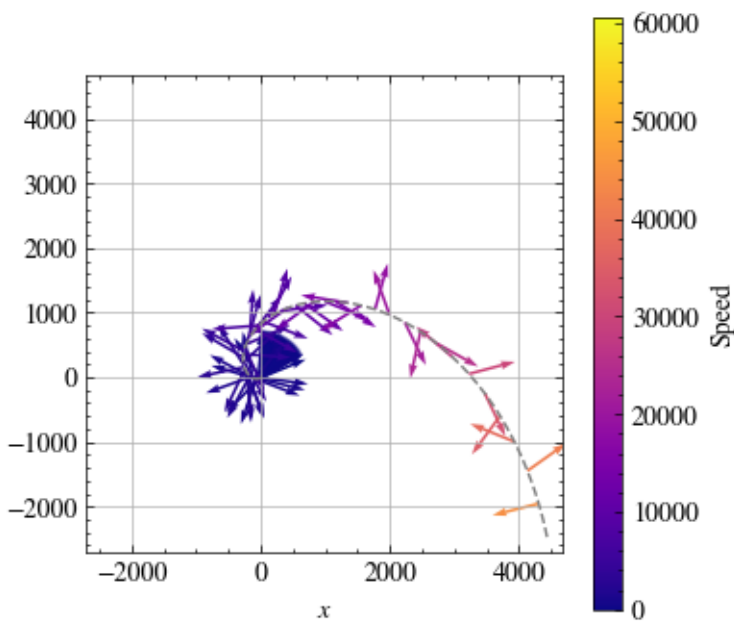


Fig. 9. Vehicle trajectory when system uses infinite-horizon LQR regulating to the equilibrium  $\bar{\mathbf{x}} = [20 \ 0 \ 0.3 \ \bar{\phi} \ 0]^T$  and has the initial conditions  $\bar{\mathbf{x}} = [15 \ 0 \ 0.3 \ \phi_{bar} \ 0]^T$ .

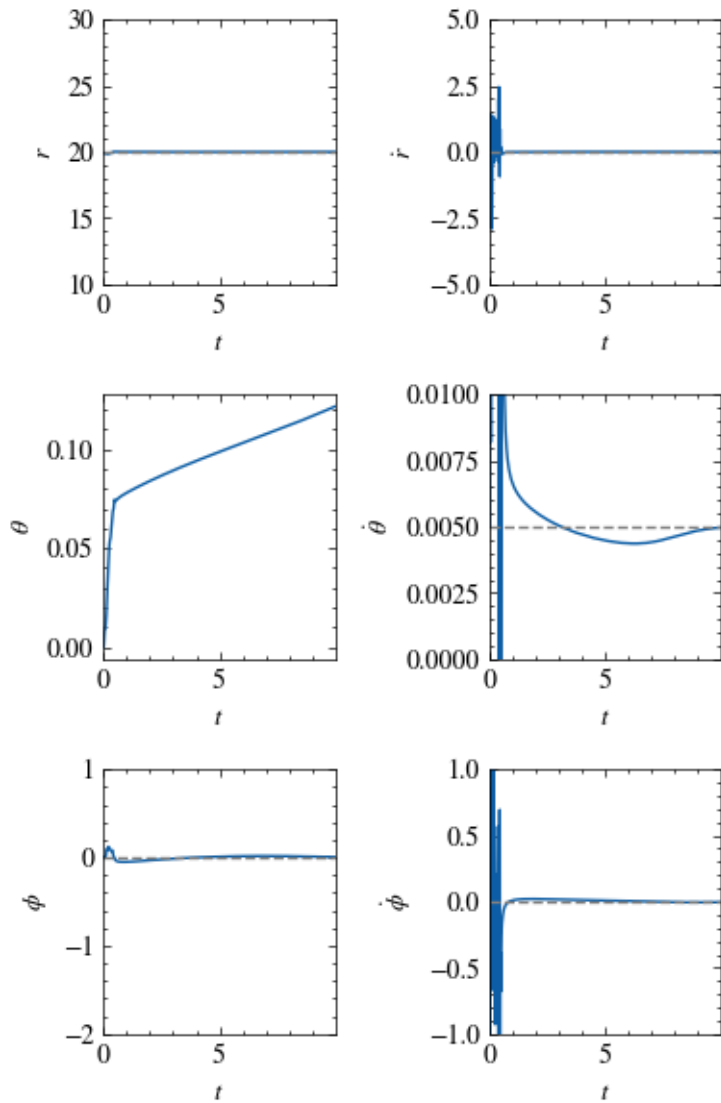


Fig. 10. Time series plots of state variables when system uses finite-horizon LQR and trajectory planning. The dashed line indicates when the system switches from trajectory following to infinite-horizon LQR.

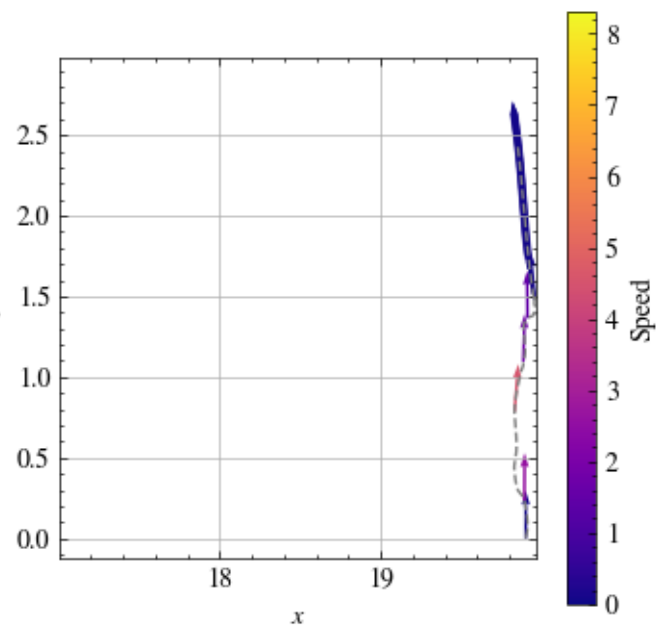


Fig. 11. Zoomed in vehicle trajectory when system uses finite-horizon LQR and trajectory planning.

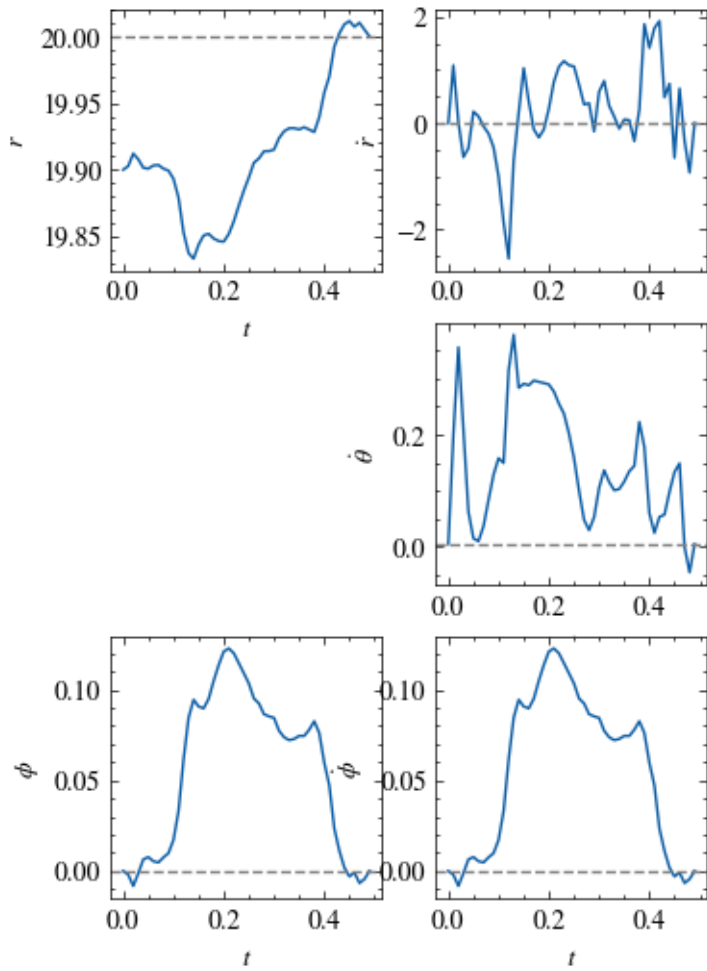


Fig. 12. Generated state trajectory using direct collocation